Original

Xi, H.; Larouche, P.; Michel, C.; Tang, S.:

Beam attenuation, scattering and backscattering of marine particles in relation to particle size distribution and composition in Hudson Bay (Canada)

Journal of Geophysical Research : Oceans (2015) AGU

DOI: 10.1002/2014JC010668

AGU PUBLICATIONS

JGR

Journal of Geophysical Research: Oceans

RESEARCH ARTICLE

10.1002/2014JC010668

Key Points:
- Attenuation and scattering variability was associated with the DCM
- Backscattering ratio was inversely related to the POM:TSM ratio
- Bulk refractive index had a larger range in PIM dominated waters

Correspondence to:
H. Xi,
hongyan.xi@hzg.de

Citation:
Xi, H., P. Larouche, C. Michel, and S. Tang (2015), Beam attenuation, scattering and backscattering of marine particles in relation to particle size distribution and composition in Hudson Bay (Canada), *J. Geophys. Res. Oceans*, *120*, 3286–3300, doi:10.1002/2014JC010668.

Received 5 JAN 2015
Accepted 13 APR 2015
Accepted article online 15 APR 2015
Published online 3 MAY 2015

Beam attenuation, scattering and backscattering of marine particles in relation to particle size distribution and composition in Hudson Bay (Canada)

Hongyan Xi[1,2], Pierre Larouche[1], Christine Michel[3], and Shilin Tang[3,4]

[1]Maurice Lamontagne Institute, Fisheries and Oceans Canada, Mont-Joli, Québec, Canada, [2]Institute of Coastal Research, Helmholtz-Zentrum Geesthacht, Geesthacht, Germany, [3]Freshwater Institute, Fisheries and Oceans Canada, Winnipeg, Manitoba, Canada, [4]South China Sea Institute of Oceanology, Chinese Academy Of Sciences, Guangzhou, People's Republic of China

Abstract This study investigated the relationships between the concentration of biogeochemical parameters and particulate beam attenuation (c_p), scattering (b_p), and backscattering (b_{bp}) in Hudson Bay. Results showed that most of the variability resulted from the presence of a deep chlorophyll maximum. c_p, b_p, and b_{bp} were all adequate proxies to estimate total suspended matter (TSM) but were mostly sensitive to particulate inorganic matter (PIM) in the surface layer, and particulate organic matter (POM) at the chlorophyll maximum depth. The backscattering ratio $\tilde{b}_{bp}$ varied in the range of 0.005–0.05 and was inversely related to the POM : TSM ratio. According to the Twardowski et al. (2001) model, the PSD slope ξ well represented $\tilde{b}_{bp}$ and bulk refractive index $\bar{n}_p$ in relation to particulate composition. For inorganic particulate dominated waters, both $\tilde{b}_{bp}$ and $\bar{n}_p$ had a larger range and a higher mean value than at organic particulate dominated waters. This knowledge on the optical properties related to the PSD and particulate composition provides valuable information for further investigation and broadens our understanding of ocean optics in high latitude waters leading to potential improvements of regional scale remote sensing algorithms.

1. Introduction

Water optical constituents (e.g., phytoplankton, dissolved organic matter and particulate matter) can be derived from remote sensing reflectance using semianalytical or analytical models. The elaboration and validation of these models depends on the knowledge of the inherent optical properties (IOPs) of suspended particles in seawater. It is generally observed that the particulate beam attenuation (c_p), scattering (b_p) and backscattering (b_{bp}) coefficients increase with increasing suspended particle concentrations. However, no single constituent clearly relates to these coefficients [*Stramski et al*., 2004] as they are driven to first order by the particle load or concentration while second-order effects are caused by size distribution, composition, refractive index, shape and internal structure of particles [*Loisel et al*., 2007; *Neukermans et al*., 2012]. Relationships between total suspended matter (TSM) and c_p, b_p or b_{bp} have been examined for both oceanic and coastal waters since 1970s [e.g., *Gibbs*, 1974; *Carder et al*., 1975]. The development of adequate instrumentation, combined with theoretical and experimental work, brought significant progress in understanding the variability of these properties [e.g., *Baker and Lavelle*, 1984; *Mikkelsen and Pejrup*, 2001; *Babin et al*., 2003; *McKee and Cunningham*, 2006; *Boss et al*., 2009; *Hill et al*., 2011]. Some studies show good correlations between b_{bp} and TSM [*Boss et al*., 2009], whereas some others find better correlations with particulate inorganic matter (PIM) [*Sun et al*., 2009; *Martinez-Vicente et al*., 2010]. These different results in various waters are mostly attributed to the composition and size distribution of particles [*Neukermans et al*., 2012].

Another essential optical parameter, the backscattering ratio $\tilde{b}_{bp}$, which is the ratio of b_{bp} to b_p, provides information on the particle type, composition and size distribution and plays an important role not only in the derivation of particles scattering phase function for water radiative transfer computations [*Mobley et al*., 2002] but is also frequently used in many semianalytical models for IOPs retrieval [*Gordon et al*., 1988; *Morel and Maritorena*, 2001]. $\tilde{b}_{bp}$ has also been used to describe the variability of the bulk refractive index $\bar{n}_p$ in various natural waters [*Twardowski et al*., 2001; *Boss et al*., 2004; *Sullivan et al*., 2005]. As $\tilde{b}_{bp}$ also depends on the relative proportion between small size and large size particles [*Ulloa et al*., 1994], an analytical model to

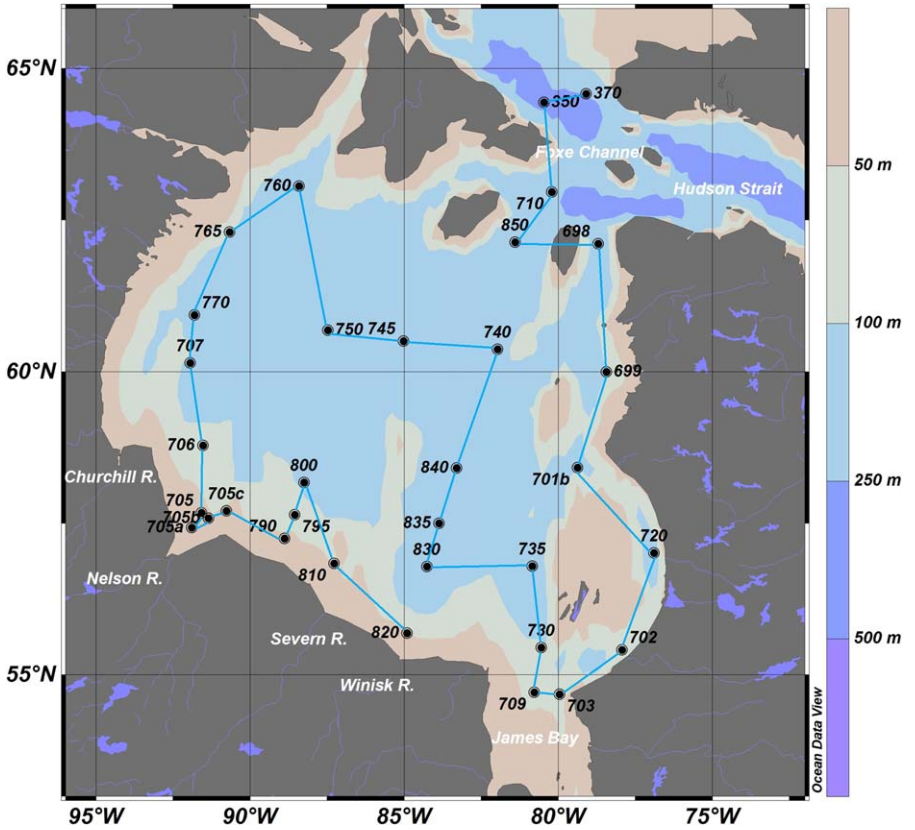

Figure 1. Study area and stations sampled. The blue line shows the sequence of stations used in other figures.

retrieve $\bar{n}_p$ from $\tilde{b}_{bp}$ and the hyperbolic slope of the particule size distribution (PSD) ξ was established by *Twardowski et al.* [2001], with expectation of lower $\bar{n}_p$ in phytoplankton dominated waters and higher $\bar{n}_p$ in mineral particle dominated waters. The PSD slope used in the *Twardowski et al.* [2001] model is often related to the spectral slope of c_p, which also exhibits an inverse power-law dependence on wavelength [*Morel*, 1973; *Boss et al.*, 2001a, 2001b; *Twardowski et al.*, 2001; *Sullivan et al.*, 2005]. The same is true of b_{bp}, though backscattering may come from a different size range of particles [*Stramski and Kiefer*, 1991; *Dall'Olmo et al.*, 2009]. There are still uncertainties for the relationship between b_{bp} spectra and the PSD [*Kostadinov et al.*, 2012] in particular in waters with complex assemblages of nonspherical, coated and aggregated particles [*Aurin et al.*, 2010].

Until now, studies in the Arctic concentrated on the description of light absorption by different constituents [*Brunelle et al.*, 2012, *Matsuoka et al.*, 2014] with some information on c_p, b_p and b_{bp} only available for the Mackenzie river plume [*Doxaran et al.*, 2012]. During an intensive sampling expedition in coastal and offshore waters in Hudson Bay (HB), we acquired a comprehensive bio-optical data set collected using multiple instruments and allowing the investigation of the regional and vertical variability of particulate beam attenuation, scattering, backscattering and backscattering ratio properties and their relations to proxies of biogeochemical parameters, such as chlorophyll *a* and suspended matter. We also assess the present inversion models by investigating the relationships between the PSD slope and $\tilde{b}_{bp}$ with respect to bulk refractive index and particulate composition.

2. Material and Methods

2.1. Study Area and Sampling

The data set used in this study was collected at 33 stations during the summer 2010 (between 9 and 31 July) ArcticNet expedition in HB (Figure 1), a large subarctic inland sea with complex water optical

properties due to a massive influx of freshwater mostly in its southern portion [*Xi et al*., 2013]. An optical profiling package was used to measure various biogeochemical, physical and optical water properties. These instruments were a WET Labs ACS measuring hyperspectral attenuation and absorption of light, a WET Labs AC9, a WET Labs ECO-BB9 to measure light backscattering by particles, a Sequoia LISST-100X to measure the size spectra of particles up to 250 μm, a Seabird SBE49 conductivity-temperature-depth (CTD) profiler to measure the vertical structure of the water column, and a WETStar chlorophyll fluorometer to measure chlorophyll fluorescence. The profiling package was slowly (0.2 m s^{-1}) lowered in the water column down to a maximum depth of 100 m. Only downcast measurements have been used to prevent interference from the instrument cage. Besides optical measurements, water samples for pigment and particle concentrations were taken at discrete depths, including the surface and the chlorophyll maximum. The surface water samples were collected using a bucket while samples at other depths were collected using a rosette system [*Xi et al*., 2014].

2.2. Attenuation, Scattering, and Backscattering Measurements

The ACS was used to measure the nonwater beam attenuation $c_{pg}(\lambda)$ and absorption coefficients $a_{pg}(\lambda)$. It has 86 spectral channels from 400 to 730 nm at a spectral resolution of about 4 nm and a measurement accuracy of $\pm$ 0.01 m^{-1}. The AC9 was equipped with a 0.2 μm filter to measure absorption by dissolved matter $a_g(\lambda)$ at 9 wavelengths (412, 440, 488, 510, 532, 555, 650, 676, and 715 nm). Prior to the field experiment, clean water and air calibration were performed to confirm that both ACS and AC9 precisions were within factory specifications. To obtain $a_{pg}(\lambda)$, $a_g(\lambda)$ and $c_{pg}(\lambda)$ from ACS and AC9 raw data, temperature and salinity corrections were performed following *Pegau et al*. [1997] and *Sullivan et al*. [2006]. Absorption coefficients $a_{pg}(\lambda)$ and $a_g(\lambda)$ were also corrected for scattering errors or remaining calibration residues by using a near infrared subtraction scheme [*Zaneveld et al*., 1994] based on the absorption at 715 nm for both ACS and AC9 data. Since the scattering by dissolved matter in water is negligible, the particulate scattering $b_p(\lambda)$ is calculated by subtracting ACS measured $a_{pg}(\lambda)$ from $c_{pg}(\lambda)$:

$$b_p(\lambda) = c_{pg}(\lambda) - a_{pg}(\lambda) \tag{1}$$

$c_{pg}(\lambda)$ data were linearly interpolated into 1 nm interval to matchup AC9 and ECO-BB9 wavelengths. The particulate attenuation coefficient $c_p(\lambda)$ was obtained by subtracting AC9 measured $a_g(\lambda)$ from ACS measured $c_{pg}(\lambda)$ at nine AC9 wavelengths:

$$c_p(\lambda) = c_{pg}(\lambda) - a_g(\lambda) \tag{2}$$

Particulate backscattering $b_{bp}(\lambda)$ was determined through estimation of the volume scattering of particles with the WET Labs ECO-BB9 at nine wavelengths (412, 440, 488, 510, 532, 595, 660, 676, and 715 nm). The instrument was calibrated by the manufacturer prior to the expedition, and data were corrected for pathlength absorption effects using the correction factor provided by the manufacturer [*McKee et al*., 2009; *Sun et al*., 2009]. The conversion from volume scattering to backscattering was performed using an *X* factor from *Boss and Pegau* [2001]. The details of the processing procedure can be found in the BB9 User's Guide. Using $b_p(\lambda)$ provided by equation (1) and $b_{bp}(\lambda)$, the backscattering ratio $\tilde{b}_{bp}(\lambda) = b_{bp}(\lambda)/b_p(\lambda)$ was calculated at the ECO-BB9 wavelengths. After correction and calculation, all absorption, attenuation, scattering and backscattering data for each vertical profile were median-binned to 1 m intervals.

2.3. PSD Measurements

The PSD were estimated from field measurements of the volume scattering function performed using a LISST-100X Type-B particle size analyzer (Sequoia, Inc). This instrument has 32 size ranges logarithmically placed from 1.25 to 250 μm in diameter (the upper size in each bin is 1.18 times the lower), with the width of individual size classes varying from 0.2 to 35 μm. Particle size and volume concentrations for each size bin were processed using the manufacturer provided software LISST-SOP [*LISST-100X Particle Size Analyzer*, 2013]. Particle number concentrations were obtained by dividing the volume concentration measured for each size bin by the volume of a sphere diameter of each size bin. A small number (5%) of PSD data contaminated by schlieren [*Mikkelsen et al*., 2008] were removed from the analysis [*Xi et al*., 2014].

The power law is the most frequently used model for optical and ecological purposes [e.g., *Jonasz*, 1983; *Bricaud et al*., 1981; *Stramski and Kiefer*, 1991], and has been theoretically justified in many studies [e.g.,

Table 1. Descriptive Statistics of Measured Parameters[a]

Variable	Units	Mean	Min	Max	S.D.	CV (%)	N
TSM	g m^{-3}	0.537	0.102	1.841	0.317	59.0	109
PIM	g m^{-3}	0.230	0.027	1.342	0.213	92.7	87
POM	g m^{-3}	0.381	0.125	1.227	0.168	44.2	87
POM : TSM		0.659	0.213	0.96	0.148	22.4	87
HPLC Chl-a	mg m^{-3}	0.776	0.077	7.056	1.262	162.7	112
$c_p(532)$	m^{-1}	0.279 (0.264)	0.096 (0.021)	0.902 (1.124)	0.161 (0.146)	57.7 (55.4)	73 (1550)
$b_p(532)$	m^{-1}	0.231 (0.191)	0.073 (0.021)	0.723 (0.909)	0.135 (0.132)	58.3 (68.9)	98 (2256)
$b_{bp}(532)$	m^{-1}	0.0035 (0.004)	0.0012 (0.0005)	0.0131 (0.033)	0.0025 (0.0038)	70.9 (95.8)	98 (2256)
$\tilde{b}_{bp}(532)$		0.015 (0.020)	0.0061 (0.0056)	0.030 (0.056)	0.0058 (0.0071)	38.6 (35.2)	98 (2256)
PSD slope, ξ		3.533 (3.628)	2.454 (2.162)	4.391 (5.066)	0.413 (0.401)	11.7 (11.1)	82 (1488)

[a]Values in parentheses represent the statistical results of the optical parameters for all binned depths from the profiling system. The mean, range (minimum and maximum), standard deviation (S.D.), variation coefficient (CV) and number of samples (*N*) for each variable are provided.

Sheldon et al., 1972; *Platt and Denman*, 1978; *Kiefer and Berwald*, 1992]. The following power law function was fitted to the PSD data:

$$N'(D)=N'(D_o)\left(\frac{D}{D_o}\right)^{-\xi}, \tag{3}$$

where D is the diameter in the center of the size class (units of μm), $N'(D)$ is the particle number density at D (units of m^{-3} μm^{-1}), D_o is a reference diameter, $N'(D_o)$ is the particle number density at D_o, and the nondimensional ξ is the PSD slope (or Junge exponent). The relative concentration of small to large particles is estimated by the PSD slope calculated by the power law model.

The LISST-100X instrument has been shown to be sensitive to the presence of particles in suspension that are finer than the measurement range of the optics [*Agrawal and Traykovski*, 2001; *Agrawal et al*., 2008; *Buonassissi and Dierssen*, 2010] leading to a raising tail at small size class. Considering this, the PSD slope ξ was calculated using equation (3) within the size range of 6.14–196 μm. This range minimized the effect of the tail at smaller size range and the very low values at the largest size classes on the slope calculation. Null data at some small size classes due to the tail were removed. A type I linear fit to the log-transformed data provided good regression results with R^2 between 0.88 and 0.99 and significant p value < 0.01 for all sampled stations (details in *Xi et al*. [2014]).

2.4. Particle and Pigment Measurements

For TSM measurements, 0.5 – 3.0 litres of sea water was filtered under low pressure onto pre-weighed 25 mm glass fiber filters (Whatman, GF/F). The filters were rinsed with Milli-Q water and kept frozen at −20°C until dried at 100°C for at least 3 h. The filters were weighted to measure the total suspended matter (TSM) concentration and burnt at 550°C for 1 h and reweighed to measure the particulate inorganic matter (PIM) concentration. The particulate organic matter (POM) concentration was calculated as POM = TSM – PIM. High-performance liquid chromatography (HPLC) was used to determine the liposoluble pigment concentrations. Samples (1.5 – 2.0 litres) were filtered onto 25 mm glass fiber filters (Whatman, GF/F), stored in cryovials and frozen in liquid nitrogen until measurement by HPLC. The samples were processed at the Horn Point Laboratory (see *Van Heukelem and Thomas* [2005] for a complete description of the methodology). HPLC Chl-a concentration is defined as the sum of chlorophyll *a* allomers and epimers, divinyl-chlorophyll *a* and chlorophyllide. The fluorescence method was also used to measure Chl-a (Fluo. Chl-a) by following the procedure proposed by *Yentsch and Menzel* [1963]. In addition, chlorophyll fluorescence (Chl fluorescence) vertical profiles were also obtained using a WETStar fluorometer. The Chl fluorescence profiles were binned into 1 m intervals.

2.5. Uncertainties in Measurements and Quality Control

The precision error of the calibrated ACS and AC9 are assumed to be within ± 0.005 m^{-1}. $a_{pg}(\lambda)$ from ACS and $a_g(\lambda)$ from AC9 were compared with laboratory absorption measurements acquired during the expedition, showing a good agreement (slope = 1.01 and R = 0.96 for $a_{pg}(\lambda)$; slope = 0.91 and R = 0.93 for $a_g(\lambda)$). Considering the relatively low scattering conditions recorded in this study (Table 1), the expected error of particulate scattering $b_p(\lambda)$ obtained by subtracting the absorption from the

attenuation are estimated to be around 18% [*Piskozub et al.*, 2004; *Martinez-Vicente et al.*, 2010]. The backscattering errors from the ECO-BB9 are assumed to be smaller than 15% of the signal based on uncertainties in backscattering coefficient conversion [*Maffione and Dana*, 1997; *Boss et al.*, 2004]. Uncertainties in the particulate backscattering ratios are likely to be less than 30%, based on the error propagation from scattering and backscattering.

Discrete measurements of TSM, PIM, and Chl-a were only estimated from single samples.Measurement noise was estimated using six blank samples (1–2 L of milli-Q water processed as a sample) for TSM and Chl-a respectively to evaluate how much error a real sample would carry due to the measurement and analysis protocols. The blank samples of TSM were also combusted to assess the error introduced to PIM by the combustion. The mean coefficient of variation (CV) of TSM measurement noise was 15%; the mean CV of PIM noise was 9.5%, while the mean CV of HPLC Chl-a noise was very small (0.49%). The Fluo Chl-a versus HPLC Chl-a were well correlated but the Fluo Chl-a was higher than HPLC Chl-a ($R = 0.97$, slope = 1.98, figure not shown). Such a high ratio has also been found in other polar environments [*Ben Mustapha et al.*, 2012; *Marrari et al.*, 2006; *Darecki et al.*, 2005]. Given their higher accuracy, HPLC Chl-a values were used to investigate their relationships with optical measurements. Chl fluorescence measured using the WETStar fluorometer were also compared with HPLC measured Chl-a values to ensure their consistency. Photoinhibition can affect the measurement of Chl fluorescence near the surface as reported in previous studies [*Cullen*, 1982; *Fennel and Boss*, 2003; *Proctor and Roesler*, 2010]. The comparison between the WETStar Chl fluorescence and discrete HPLC Chl-a values showed that they were in good agreement ($R = 0.84$, $p < 0.001$). There were no differences between WETStar fluorescence and HPLC Chl-a values in the mixed layer (mean MLD = 15 m) and at the depth of chlorophyll maximum. In the present study the WETStar Chl fluorescence was only used to show the vertical variation of chlorophyll, but was not involved in the analysis of any bio-optical relationships.

3. Results and Discussion

3.1. Distribution of Biogeochemical Parameters and Optical Variables

HB has a lower average salinity level than ocean waters due to the large volume of terrestrial freshwater runoff entering the bay and the limited connections with the Atlantic Ocean. Figure 2 shows that HB stratification was mostly driven by salinity. Vertical temperature differences were always relatively small ($\sim$1°C) while strong salinity gradients could be observed. The mixed layer depth (MLD) ranged from a maximum of 30 m to a minimum of 8 m with a mean value of 15 m [*Xi et al.*, 2013]. The stratification results from the impact of many important rivers injecting large amounts of freshwater in the Bay. The most important impact was observed at the entrance of James Bay (St. 703) where the lowest salinities and temperature were measured. The lense of freshwater originating from James Bay impacted a large area extending west of the Belcher Islands up to St. 699 as observed before [*Harvey et al.*, 2001]. The vertical extent of the freshwater lense slowly decreased from $\sim$20 m in James Bay to $\sim$5 m at St. 699. Other areas were also affected by freshwater such as near the Nelson River (St. 705) and the Winisk River (St. 820). The freshwater influence was however confined to a relatively small band along the southern shore as indicated by the higher salinity and temperature observed at stations 790 and 795. Except for these areas highly impacted by freshwater inputs, the rest of HB showed a relatively small stratification. Along an East to West transect (Sts. 699, 740, 745, 750, 770), there was gradual decrease of stratification. The relatively low salinities observed in the center of the Bay (Sts. 745 and 750) supported the model results of *St. Laurent et al.* [2011] showing a transfer of freshwater toward the interior of Hudson Bay by Ekman transport.

Figure 3a shows the vertical structure of Chl-a, as evaluated by chlorophyll fluorescence. Low levels of Chl-a were measured in the surface layer except at St. 703 at the entrance of James Bay and St. 705a near the Nelson River. Our HPLC measurements showed that the surface Chl-a concentrations were very low with the range of 0.077–0.441 mg m^{-3} and a mean of 0.184 mg m^{-3}, indicating that there was no surface phytoplankton blooms detected during the cruise in July [*Xi et al.*, 2013]. The highest values were observed at the depth of the chlorophyll maximum (DCM) located between 20 m and 75 m, always below the first optical depth (i.e., the layer over which light attenuates to $\sim$37% of its magnitude at the surface) [*Werdell et al.*, 2013] that was 9.8 m on average. Stations in the north of the Bay (e.g., Sts. 370 – 698) had shallower DCM (25 – 50 m) compared to other offshore stations (e.g., St. 735 – 707 and St. 800) (40 – 75 m). The intensity of

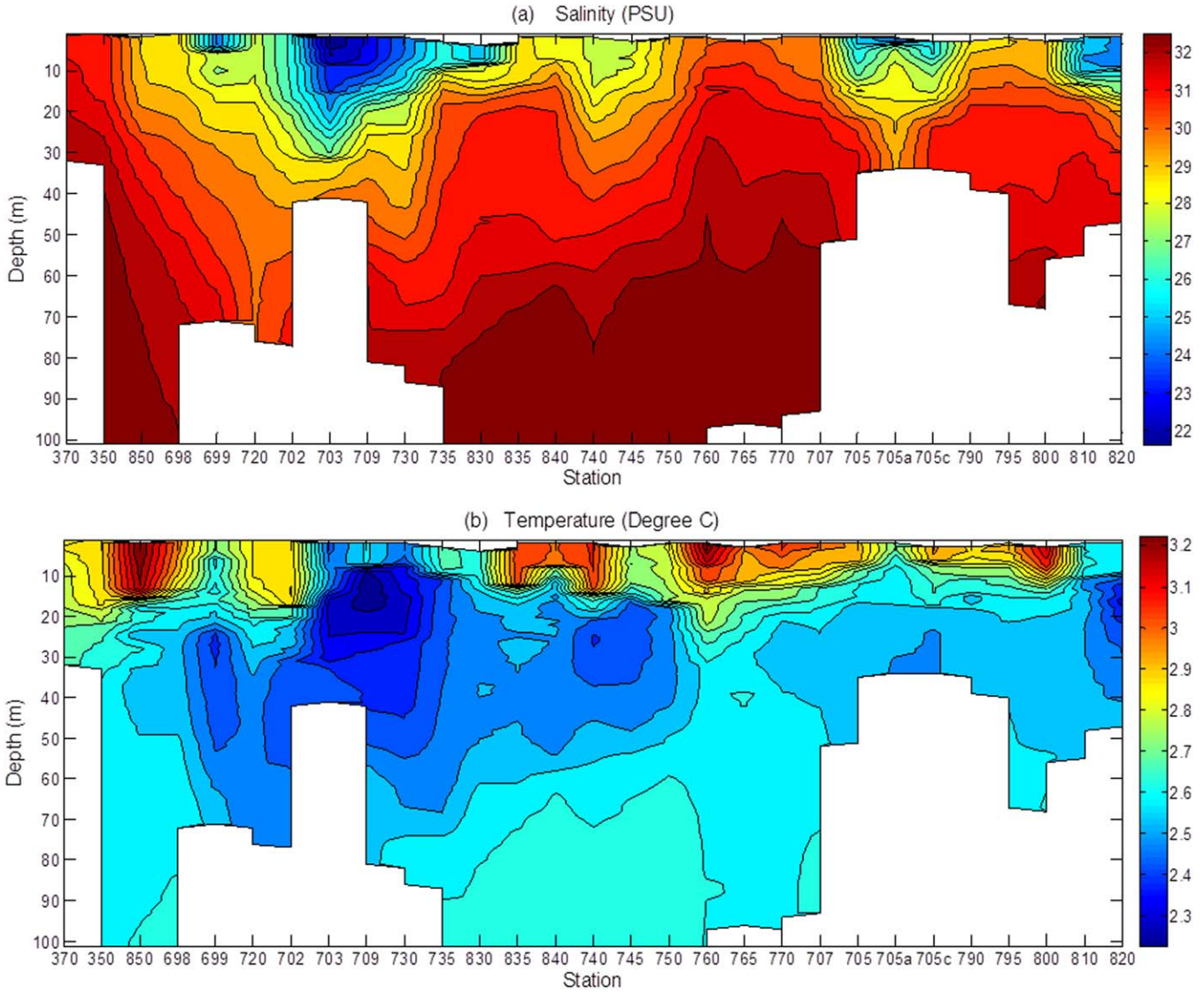

Figure 2. Vertical variation of (a) temperature and (b) salinity in HB from available CTD profiles (refer to Figure 1 for the station sequence).

the DCM was also variable with higher values observed at the offshore stations. St. 698 showed a strong uplift of the DCM (~15 m) consistent with the smaller vertical stratification observed (Figure 2a).

Table 1 shows that the mean TSM value, measured from discrete samples, was relatively low (0.54 ± 0.32 g m^{-3}). Figure 3b shows that there was little vertical variation of TSM. Maximums were observed at the surface of St. 705b near Nelson River and at the entrance of James Bay (Sts. 703, 709), consistent with higher suspended material near freshwater sources. Surface TSM values were also found negatively correlated with the surface salinity ($R^2 = 0.22$, $p < 0.01$), supporting that the freshwater flow contributed significantly to the surface sediment loads. Higher TSM concentrations were also observed at the DCM, leading to a positive correlation with Chl-a. Suspended matter analysis showed an overall higher proportion of organic particles (66%) than inorganic particles (34%).

Figure 4 shows the vertical variation of $c_p(532)$ at the 22 available stations. $c_p(532)$ spanned a range of 0.021–1.124 m^{-1} with an average of 0.264 ± 0.146 m^{-1}. In the surface layer, higher beam attenuation was measured at the James Bay entrance (St. 703), Nelson River Estuary (St. 705a) and St. 698. Below the surface layer, the location of maximum $c_p(532)$ values were in agreement with the DCM. However higher $c_p(532)$

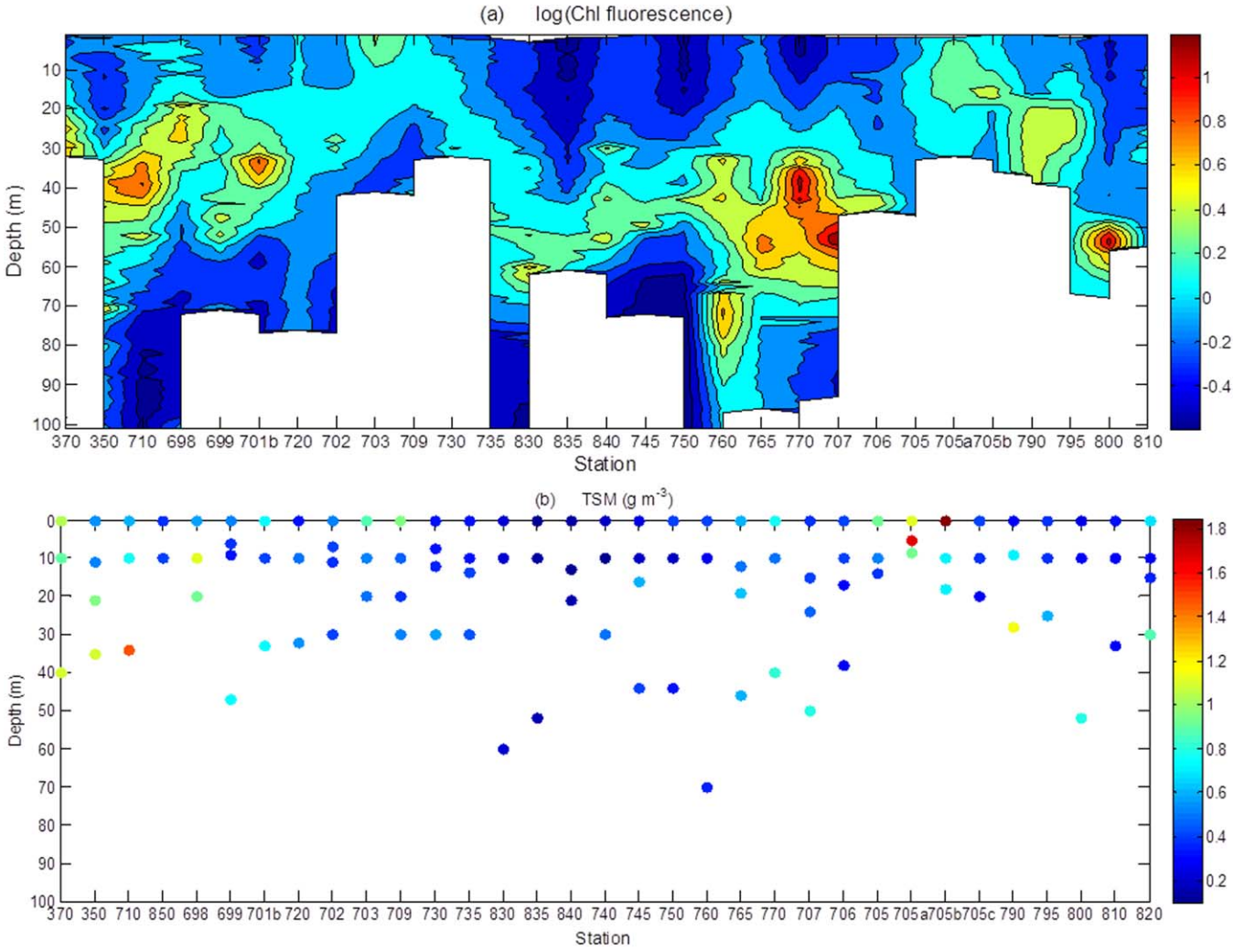

Figure 3. Vertical variation of (a) chlorophyll fluorescence from the WETStar fluorometer (29 stations) and (b) TSM concentrations at discrete depths. A base-10 logarithm was applied to Chl fluorescence to better show the structure.

were also found at the bottom layer of several stations (e.g., Sts.698, 720, 703, and 765) probably due to the resuspension of smaller particles as the profiling package was close to the bottom, where phytoplankton biomass was low [*Xi et al*., 2014]. With exception of the bottom layer values at these stations, $c_p(532)$ values were well correlated with Chl fluorescence values ($R = 0.78$). The lowest $c_p(532)$ were observed in the central part of the bay (i.e., St. 745 and 750) indicating very low biomass and particle concentration. Different from other stations, the surface layer of St. 698 showed an abnormal pattern with higher c_p and b_p but lower Chl-a and TSM concentrations. HPLC results showed that microplankton represented 68% of the phytoplankton community, close to the mean value of all stations, which was 62% according to *Xi et al*. [2014]. However the PSD measurements showed that the PSD slope was only 3.38, indicating the presence of more large particles. The slope-derived microplankton contribution was $\sim$ 80% [*Xi et al*., 2014], explaining the observed higher scattering even though there was a lower biomass.

Figure 5 shows the vertical variation of the particle scattering coefficient, backscattering coefficient, and backscattering ratio at 532 nm for the 29 available stations. $b_p(532)$ range was 0.1–0.9 m^{-1} with an average of 0.19 $\pm$ 0.13 m^{-1}, and $b_{bp}(532)$ range was 0.001–0.03 m^{-1} with an average of 0.004 $\pm$ 0.004 m^{-1} (Table 1). Both b_p and b_{bp} values were relatively low compared to other coastal waters such as the Monterey Bay [*Snyder et al*., 2008], the Adriatic Sea [*Berthon et al*., 2007], the coastal waters of the Black Sea [*Chami et al*., 2005], or the English Channel [*Martinez-Vicente et al*., 2010]. The distribution of $b_p(532)$ was consistent with

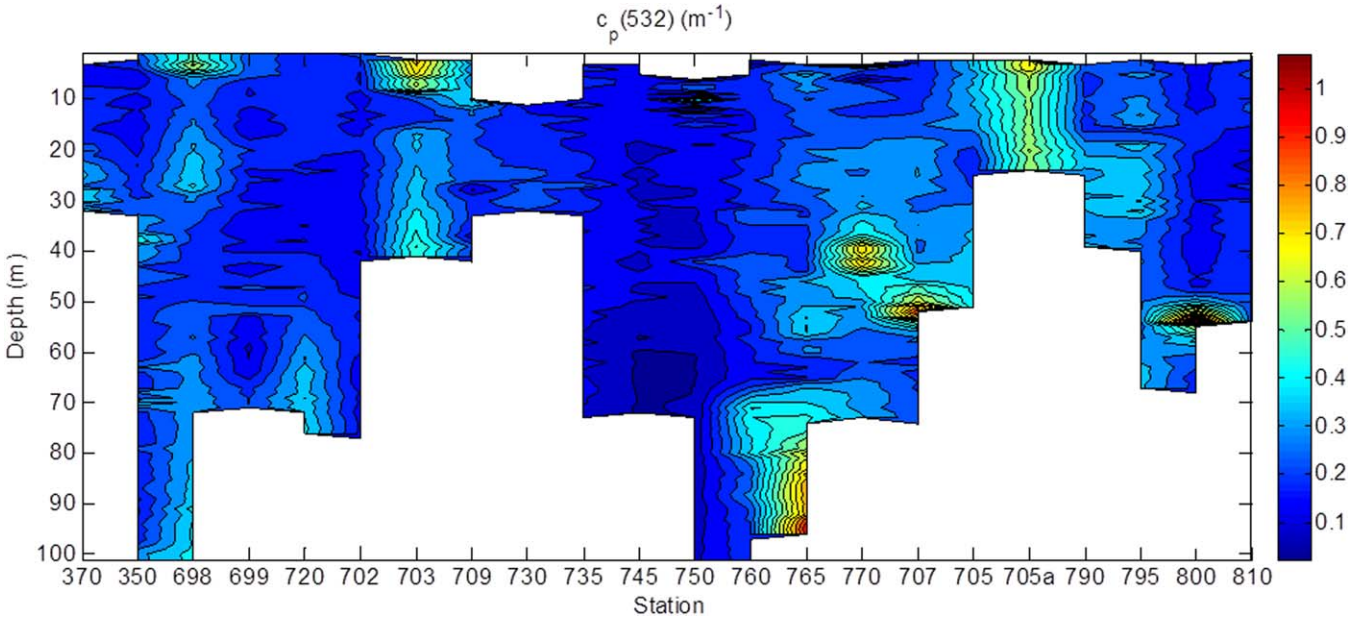

Figure 4. Vertical variation of particulate beam attenuation at 532 nm $c_p(532)$.

the one of $c_p(532)$ (Figure 4) with an R of 0.96 (Table 2). Even though the general distribution of $b_{bp}(532)$ was consistent with the one of $b_p(532)$, some differences must be noted. The $b_p(532)$ maxima observed at the surface of Sts. 703 and 698 did not correspond to similar maxima for $b_{bp}(532)$. Despite these exceptions, $b_{bp}(532)$ was generally well correlated to $b_p(532)$ and $c_p(532)$ with R of 0.75 and 0.74, respectively (Table 2).

The overall mean backscattering ratio $\tilde{b}_{bp}$ at 532 nm was 0.02 ± 0.007. The range of $\tilde{b}_{bp}$ (0.005–0.05) covered nearly the whole range observed in previous studies performed in different coastal, oceanic, and lake environments [*Twardowski et al*., 2001; *Chang et al*., 2006; *Boss et al*., 2004; *McKee and Cunningham*, 2006; *Loisel et al*., 2007; *Whitmire et al*., 2007; *Snyder et al*., 2008; *Sun et al*., 2009]. Figure 5c shows that $\tilde{b}_{bp}(532)$ increased with depth with the highest values often observed near the bottom. This is consistent with the observations by *Chami et al*. [2005] but the HB values spanned a larger range. The mean ratio at the surface layer was only 0.013 compared to 0.023 for the deeper waters (below 30 m). Higher $\tilde{b}_{bp}(532)$ values near the bottom are probably associated to the resuspension of small mineral particles [*Xi et al*., 2014] as suggested by the negative correlation between $\tilde{b}_{bp}(532)$ and the POM : TSM ratio (Table 2). $\tilde{b}_{bp}$ is also an indicator of the relative proportion between small size and large size particles with higher proportion of small size particles resulting in higher $\tilde{b}_{bp}$ [*Ulloa et al*., 1994; *Loisel et al*., 2007]. *Xi et al*. [2014] showed that in deep waters of HB, the proportion of small size particles were higher, in good agreement with the higher $\tilde{b}_{bp}$ in deep waters.

3.2. Optical Variables in Relation to Biogeochemical Parameters

Table 3 shows that TSM was significantly correlated, with the three optical variables ($b_p(532)$, $b_{bp}(532)$ and $c_p(532)$), and that the relationships showed little difference for values at different depths. $b_{bp}(532)$ showed a significant correlation with TSM ($R^2 = 0.56$) indicating that the backscattering coefficient is a good first-order parameter to estimate TSM in bio-optical models. PIM values were also well correlated with the three optical variables, and the highest R^2 also occurred with $b_{bp}(532)$. POM values were better correlated with b_p, b_{bp} and c_p at the DCM than at other depths. This probably results from the large contribution of POM to TSM ($> 70\%$) at the DCM. Among the three optical variables, b_{bp} appears as the best proxy to describe the suspended matter having always the highest R^2 as indicated previously by *Boss et al*. [2009]. Although the relationship was poor due to a large scatter, a negative trend was found between the POM : TSM ratio and the three optical variables showing that the relative amount of organic material affects the scattering, backscattering and the attenuation properties to a certain extent. This explains why $\tilde{b}_{bp}$ was poorly correlated

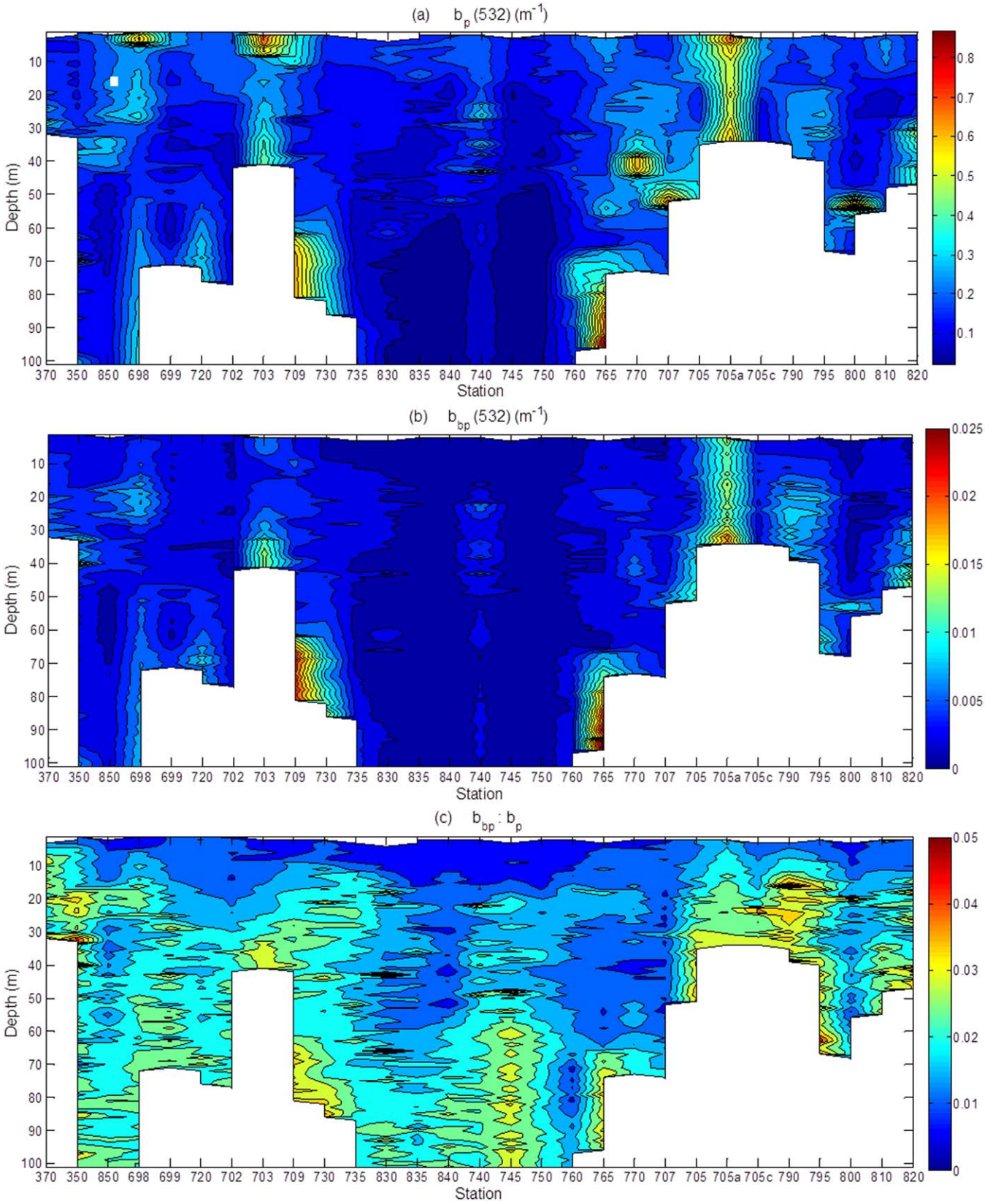

Figure 5. Vertical variation of (a) b_p (532), (b) b_{bp}(532), and (c) $\tilde{b}_{bp}$.

Table 2. Correlation Coefficients (*R*) Between Optical Measurements and Biogeochemical Parameters at Discrete Depths[a]

	PIM	TSM	POM	POM : TSM	HPLC Chl-a	Fluo. Chl-a	$b_p(532)$	$b_{bp}(532)$	$\tilde{b}_{bp}$
TSM	0.86*								
POM	0.31	0.76 *							
POM : TSM	−0.80*	−0.50 *	0.10						
HPLC Chl-a	0.10	0.49 *	0.78*	0.14					
Fluo. Chla	0.14	0.54 *	0.79*	0.17	0.97*				
$b_p(532)$	0.46*	0.57 *	0.42	−0.30	0.37	0.31			
$b_{bp}(532)$	0.68*	0.75 *	0.48*	−0.50*	0.46*	0.41	0.75*		
$\tilde{b}_{bp}$	0.28	0.25	−0.20	−0.48*	0.12	0.16	−0.10	0.54*	
$c_p(532)$	0.39	0.52 *	0.45	−0.25	0.45	0.42	0.96*	0.74*	−0.05

[a]Significant correlation (p value < 0.01) is marked with an asterisk.

with other biogeochemical parameters but had an significant inverse relationship with POM : TSM ratio (Table 2).

Table 3 shows that significant positive relationships between optical variables and Chl-a only took place at the DCM with Chl-a explaining 39%, 47% and 34% of the variation of b_p, b_{bp} and c_p, respectively. This indicates that the attenuation, scattering and backscattering properties can be related to chlorophyll concentration only at optical depths where the living organic material and phytoplankton are dominating the total suspended material. Otherwise, pigments only have little influence on these optical properties.

Figure 6a shows the backscattering ratio, $\tilde{b}_{bp}$ as a function of Chl-a. Unlike inverse relationships reported in previous studies [*Loisel et al*., 2007; *Sun et al*., 2009], the correlation between $\tilde{b}_{bp}$ and Chl-a was weak in HB (R = 0.12, Table 2). About half of the $\tilde{b}_{bp}$ values were higher than empirical [*Twardowski et al*., 2001; *Sullivan et al*., 2005; *Whitmire et al*., 2007] and semianalytical relationships [*Ulloa et al*., 1994; *Morel and Maritorena*, 2001] with no difference observed between the different depths. Similar results have been reported by *Chami et al*. [2005] for coastal waters of the Black Sea where inorganic particles are dominant and influence the scattering and backscattering coefficients. In our study, the organic particles constituted, on average, more than 60% of TSM, a very different case from *Chami et al*. [2005]. The lack of correlation between the Chl-a and $\tilde{b}_{bp}$ at low Chl-a concentrations has also been reported before [*Whitmire et al*., 2007; *Twardowski et al*., 2001; *Sullivan et al*., 2005] as other particles contribute strongly to the magnitude of $\tilde{b}_{bp}$. Several points (circled in Figure 6a), located under the surface (10 m) or near the DCM, showed both higher $\tilde{b}_{bp}$ and Chl-a, contributing to the poor relationship between Chl-a and $\tilde{b}_{bp}$. The PSD slope values at these points were relatively high ($\xi > 3.60$), confirming the relative dominance of small size particles that results in higher $\tilde{b}_{bp}$ [*Ulloa et al*., 1994; *Loisel et al*., 2007]. Chl-a is thus not an ideal descriptor of $\tilde{b}_{bp}$ in the HB. This is

Table 3. Determination Coefficient (R^2), p Value (p) and Observation Numbers (N) of the Least Square Regression Relationships Between Optical Variables and Biogeochemical Parameters[a]

	$b_p(532)$			$b_{bp}(532)$			$c_p(532)$		
	R^2	p	N	R^2	p	N	R^2	p	N
TSM (all)	0.32	< 0.01*	98	0.56	< 0.01*	98	0.27	< 0.01*	73
TSM (non-DCM)	0.36	< 0.01*	74	0.52	< 0.01*	74	0.34	< 0.01*	56
TSM (DCM)	0.26	< 0.01*	24	0.63	< 0.01*	24	0.17	< 0.05	17
PIM (all)	0.20	< 0.05	87	0.45	< 0.01*	87	0.15	< 0.05	73
PIM (non-DCM)	0.44	< 0.01*	65	0.58	< 0.01*	65	0.40	< 0.01*	56
PIM (DCM)	0.00		22	0.24	< 0.01*	22	0.00		17
POM (all)	0.17	< 0.05	87	0.23	< 0.01*	87	0.21	< 0.03	73
POM (non-DCM)	0.06	0.11	65	0.10	< 0.10	65	0.08	0.10	56
POM (DCM)	0.39	< 0.01*	22	0.54	< 0.01*	22	0.34	< 0.01*	17
POM : TSM (all)	0.10	0.07	87	0.23	< 0.01*	87	0.07	0.10	73
POM : TSM (non-DCM)	0.36	< 0.01*	65	0.40	< 0.01*	65	0.32	< 0.01*	56
POM : TSM (DCM)	0.04		22	0.06	= 0.12	22	0.02		17
Chl-a (all)	0.14	< 0.05	98	0.21	< 0.01*	98	0.20	< 0.05	73
Chl-a (non-DCM)	0.01		74	0.13	= 0.05	74	0.00		56
Chl-a (DCM)	0.39	< 0.01*	24	0.47	< 0.01*	24	0.34	< 0.01*	17

[a]Significant correlation (p value < 0.01) is marked with an asterisk.

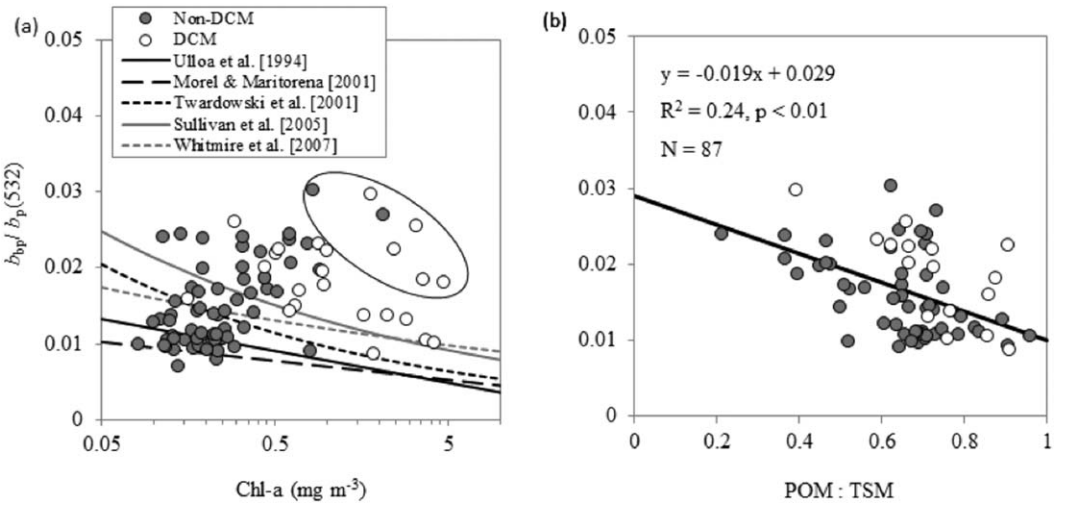

Figure 6. Scatterplot of $\tilde{b}_{bp}$ at 532 nm as a function of (a) Chl-a concentrations and (b) POM:TSM ratio. The solid line and equation in Figure 6b shows the linear fit to the whole data set. Points circled in Figure 6a showing higher $\tilde{b}_{bp}$ and Chl-a are discussed in the text.

also confirmed by the weak relationship between $\tilde{b}_{bp}$ and Chl-a : c_p ratio (not shown), which can often be considered as an indicator of the nature of bulk particulate matter [*Loisel and Morel*, 1998; *Loisel et al*., 2007]. Figure 6b shows that $\tilde{b}_{bp}$ decreased when the proportion of POM increased. This is consistent with the results from *Neukermans et al*. [2012] and agrees with expectations of lower $\tilde{b}_{bp}$ for particles dominated by organic matter and higher $\tilde{b}_{bp}$ for inorganic particles [*Loisel et al*., 2007].

The bulk refractive index, $\bar{n}_p$, is another important parameter in optical modeling that is used to characterize phytoplankton carbon stocks [*Behrenfeld et al*., 2005; *Kostadinov et al*., 2009]. $\bar{n}_p$ can be determined according to an analytical model developed by *Twardowski et al*. [2001]:

$$\bar{n}_p = 1 + \tilde{b}_{bp}^{\,0.5377+0.4867(\xi-3)^2}\left[1.4676 + 2.2950(\xi-3)^2 + 2.3113(\xi-3)^4\right] \quad (4)$$

Figure 7 shows that $\bar{n}_p$ estimated by equation (4) using our measurements of $\tilde{b}_{bp}$ and the PSD slope were in the 1.00–1.24 range. Previous studies showed that particle size and composition influence $\bar{n}_p$ [*Ulloa et al*., 1994] with large organic particles having an index of refraction around 1.05 because of their high water content [*Carder et al*., 1972; *Aas*, 1996; *Stramski*, 1999], whereas mineral particles have an index as high as 1.26 [*Twardowski et al*., 2001; *Woźniak and Stramski*, 2004]. Previous studies also indicated that $\bar{n}_p$ may exhibit a relatively large variability (strong scatter of the $\bar{n}_p$ points) even if the proportion between inorganic and organic particles is constant [*Loisel et al*., 2007], as the particle shape and structure may also affect optical properties [*Neukermans et al*., 2012]. The observed range of HB values thus appear reasonable, covering both coastal and offshore waters and in agreement with a mixture of organic and mineral particles. Figure 7 shows that $\bar{n}_p$ values were higher (1.14–1.22) at high PIM : TSM ratios and lower (1.02 – 1.18) at low PIM : TSM ratios. This is consistent with previous studies about particulate composition for both Case I and Case II waters [*Twardowski et al*., 2001; *Loisel et al*., 2007; *Sun et al*., 2009] and indicates that particulate

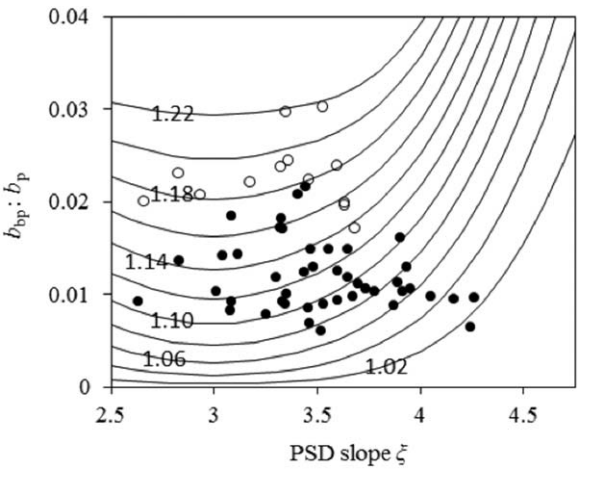

Figure 7. Particulate backscattering ratio $\tilde{b}_{bp}$ versus PSD slope ξ. The solid curves overlaid represent the refractive index $\bar{n}_p$ contours as calculated by the model of *Twardowski et al*. [2001]. The open circles and dots represent the sets of data with the PIM:TSM > 0.5 and PIM:TSM ≤ 0.5, respectively.

composition conditions the bulk refractive index variability in HB. It should however be noted that some of the variability observed in Figure 7 can also be explained by the presence of diatoms having silica frustules that can have a high PIM:TSM ratio but a low refractive index.

4. Conclusion

Using a unique set of optical and biogeochemical measurements collected in Hudson Bay, we were able to develop a better understanding of the particles attenuation, scattering and backscattering properties in arctic waters. Results showed that most of the optical variables and biogeochemical parameters variability was associated with the presence of the DCM. Local sources of freshwater have a strong but spatially limited effect on optical properties related to particles. The spectral dependency of backscattering, which may be assessed qualitatively form satellite observations of ocean color [*Loisel et al*., 2006], is sensitive to the PSD. *Kostadinov et al*. [2009] proposed a novel bio-optical algorithm to retrieve the parameters of the power law PSD by means of satellite derived b_{bp} and Mie modeling. Theoretical and experimental studies also showed that the PSD slope ξ can be estimated from the spectral dependency of the particulate beam attenuation c_p [*Morel*, 1973; *Boss et al*., 2001b] indicating that there might be a chance to understand the spectral dependency of c_p from satellite measurements by using the quantitative relationship between the ξ and c_p slopes. To reach that goal, the spectral dependency of backscattering and attenuation are first to be fully understood and the uncertainties existing in the relationships with the PSD, should be investigated in future studies.

Relationships between optical properties and biogeochemical parameters in HB showed the variation of bio-optical relations due to the change in particle composition. Compared to scattering $b_p(532)$ and attenuation $c_p(532)$, backscattering $b_{bp}(532)$ is the most suitable proxy that can be used to estimate TSM and PIM concentrations within the first optical depth leading the way for a potential remote sensing algorithm. As Chl-a in the surface layer is well correlated to the absorption property in Hudson bay [*Xi et al*., 2013], combining all these regional relationships can provide valuable baseline information about Hudson Bay surface waters. Considering the difficulty to get access to the area using ships, remote sensing might be the only way to improve our knowledge of Hudson Bay ecology in a context of an increasingly longer open water season [*Galbraith and Larouche*, 2011].

Overall, this study provided general knowledge of the optical properties and helped to evaluate the sensitivity of the inherent optical properties measured in situ, with regard to the biogeochemical parameters and the nature of the particulate composition and size in Arctic waters. Given the high variability observed in Hudson Bay, current empirical bio-optical algorithms are likely to be inapplicable to the study area. Efforts should now be put on the development of more sophisticated remote sensing algorithms with full consideration of known optical properties in high latitude waters.

Notation

$a_g(\lambda)$	absorption coefficient of CDOM measured by AC9, m^{-1}.
$a_{pg}(\lambda)$	nonwater absorption measured by ACS, m^{-1}.
$b_p(\lambda)$	particulate scattering coefficient measured by ACS, m^{-1}.
$b_{bp}(\lambda)$	particulate backscattering coefficient measured by ECO BB9, m^{-1}.
$\tilde{b}_{bp}$	backscattering ratio, $b_{bp}(\lambda)/b_p(\lambda)$.
CDOM	colored dissolved organic matter.
DCM	depth of chlorophyll maximum, m.
$c_{pg}(\lambda)$	nonwater beam attenuation measured by ACS, m^{-1}.
$c_p(\lambda)$	particulate beam attenuation coefficient measured by AC meters, m^{-1}.
Fluo. Chl-a	chlorophyll *a* concentration measured with fluorescence method, mg m^{-3}.
HPLC Chl-a	chlorophyll *a* concentration measured with HPLC, mg m^{-3}.
Chl fluorescence	chlorophyll fluorescence from WETStar.
ξ	Junge slope of the particle size distribution (PSD).
λ	wavelength, nm.

MLD	mixed layer depth, m.
$N(D)$	particle number concentration at size class D, m^{-3}.
$N'(D)$	particle number density at size class D, $m^{-3}\ \mu m^{-1}$.
$\bar{n}_p$	bulk refractive index.
PIM	particulate inorganic matter, g m^{-3}.
POM	particulate organic matter, g m^{-3}.
PSD	particle size distribution.
TSM	total suspended matter, g m^{-1}.

Acknowledgments
We thank the two anonymous reviewers for their constructive comments on the manuscript. This work was made possible with the support of the Natural Sciences and Engineering Research Council of Canada (NSERC), the Department of Fisheries and Oceans Canada and the Canadian Space Agency. We are grateful to the crew of the NGCC Amundsen during the 2010 ArcticNet expedition for their dedication supporting science activities. We acknowledge the important contribution of Michel Gosselin who provided chlorophyll concentrations measured using fluorescence method. Data to support this article are available upon request from Pierre Larouche (Pierre.Larouche@dfo-mpo.gc.ca).

References

Aas, E. (1996), Refractive index of phytoplankton derived from its metabolite composition, *J. Plankton Res.*, *18*, 2223–2249.
Agrawal, Y., and P. Traykovski (2001), Particles in the bottom boundary layer: Concentration and size dynamics through events, *J. Geophys. Res.*, *106*, 9533–9542, doi:10.1029/2000JC900160.
Agrawal, Y., A. Whitmire, O. Mikkelsen, and H. Pottsmith (2008), Light scattering by random shaped particles and consequences on measuring suspended sediments by laser diffraction, *J. Geophys. Res.*, *113*, C04023, doi:10.1029/2007JC004403.
Aurin, D., H. M. Dierssen, M. S. Twardowski, and C. S. Roesler (2010), Optical complexity in Long Island Sound and implications for coastal ocean color remote sensing, *J. Geophys. Res.*, *115*, C07011, doi:10.1029/2009JC005837.
Babin, M., A. Morel, V. Fournier-Sicre, F. Fell, and D. Stramski (2003), Light scattering properties of marine particles in coastal and open ocean waters as related to the particle mass concentration, *Limnol. Oceanogr. Methods*, *48*, 843–859.
Baker, E. T., and J. W. Lavelle (1984), The effect of particle size on the light attenuation coefficient of natural suspensions, *J. Geophys. Res.*, *89*, 8197–8203, doi:10.1029/JC089iC05p08197.
Behrenfeld, M. J., E. Boss, D. A. Siegel, and D. M. Shea (2005), Carbon-based ocean productivity and phytoplankton physiology from space, *Global Biogeochem. Cycles*, *19*, GB1006, doi:10.1029/2004GB002299.
Ben Mustapha, S., S. Bélanger, and P. Larouche (2012), Evaluation of ocean color algorithms in the southeastern Beaufort Sea, Canadian Arctic: New parametrization using SeaWiFS, MODIS and MERIS spectral bands, *Can. J. Remote Sens.*, *38*(5), 1–22.
Berthon, J. F., E. Shybanov, E., M. E. G. Lee, and G. Zibordi (2007), Measurements and modeling of the volume scattering function in the coastal northern Adriatic Sea, *Appl. Opt.*, *46*, 5189–5203.
Boss, E., and W. S. Pegau (2001), The relationship of light scattering at an angle in the backward direction to the backscattering coefficient, *Appl. Opt.*, *40*, 5503–5507.
Boss, E., W. S. Pegau, W. D. Gardner, R. V. Zaneveld, A. H. Barnard, M. S. Twardowski, G. C. Chang, and T. D. Dickey (2001a), Spectral particulate attenuation and particle size distribution in the bottom boundary layer of a continental shelf, *J. Geophys. Res.*, *106*, 9509–9516.
Boss, E., M. S. Twardowski, and S. Herring (2001b), Shape of the particulate beam attenuation spectrum and its inversion to obtain the shape of the particulate size distribution, *Appl. Opt.*, *40*, 4885–4893.
Boss, E., W. S. Pegau, M. Lee, M. Twardowski, E. Shybanov, G. Korotaev, and F. Baratange (2004), Particulate backscattering ratio at LEO 15 and its use to study particle composition and distribution, *J. Geophys. Res.*, *109*, C01014, doi:10.1029/2002JC001514.
Boss, E., et al. (2009), Comparison of inherent optical properties as a surrogate for particulate matter concentration in coastal waters, *Limnol. Oceanogr. Methods*, *7*, 803–810.
Bricaud, A., A. Morel, and L. Prieur (1981), Absorption by dissolved organic matter of the sea (yellow substance) in the UV and visible domains, *Limnol. Oceanogr.*, *26*, 43–53, doi:10.4319/lo.1981.26.1.0043.
Brunelle, C. B., P. Larouche, and M. Gosselin (2012), Variability of phytoplankton light absorption in Canadian Arctic Seas, *J. Geophys. Res.*, *117*, C00G17, doi:10.1029/2011JC007345.
Buonassissi, C. J., and H. M. Dierssen (2010), A regional comparison of particle size distributions and the power law approximation in oceanic and estuarine surface waters, *J. Geophys. Res.*, *115*, C10028, doi:10.1029/2010JC006256.
Carder, K. L., R. D. Tomlinson, and G. F. Beardsley Jr. (1972), A technique for the estimation of indices of refraction of marine phytoplankters, *Limnol. Oceanogr.*, *17*, 833–839.
Carder, K. L., J. Beardsley, F. George, and H. Pak (1975), Physical, chemical and optical measures of suspended-particle concentrations: Their intercomparison and application to the West African Shelf, *Suspended Solids Water*, *4*, 173–193.
Chami, M., E. B. Shybanov, T. Y. Churilova, G. A. Khomenko, M. E. G. Lee, O. V. Martynov, G. A. Berseneva, and G. K. Korotaev (2005), Optical properties of the particles in the Crimea coastal water (Black Sea), *J. Geophys. Res.*, *110*, C11020, doi:10.1029/2005JC003008.
Chang, G. C., A. H. Barnard, S. McLean, P. J. Egli, C. Moore, J. R. V. Zaneveld, T. D. Dickey, and A. Hanson (2006), In situ optical variability and relationships in the Santa Barbara Channel: Implications for remote sensing, *Appl. Opt.*, *45*, 3593–3604, doi:10.1364/AO.45.003593.
Cullen, J. J. (1982), The deep chlorophyll maximum: Comparing vertical profiles of chlorophyll a, *Can. J. Fish. Aquat. Sci. 39*, 791–803.
Dall'Olmo, G., T. K. Westberry, M. J. Behrenfeld, E. Boss, and W. H. Slade (2009), Significant contribution of large particles to optical backscattering in the open ocean, *Biogeosciences*, *6*, 947–967.
Darecki, M., S. Kaczmarek, and J. Olsweski (2005), SeaWiFS ocean colour chlorophyll algorithms for the southern Baltic sea, *Int. J. Remote Sens.*, *26*, 247–260.
Doxaran, D., J. Ehn, S. Bélanger, A. Matsuoka, S. Hooker, and M. Babin (2012), Optical characterisation of suspended particles in the Mackenzie River plume (Canadian Arctic Ocean) and implications for ocean colour remote sensing. *Biogeosciences*, *9*, 3213–3229.
Fennel, K., and E. Boss (2003), Subsurface maxima of phytoplankton and chlorophyll: Steady-state solutions from a simple model, *Limnol. Oceanogr. Methods*, *48*, 1521–1534.
Galbraith, P. S., and P. Larouche (2011), Sea-surface temperature in Hudson Bay and Hudson Strait in relation to air temperature and ice cover breakup, 1985–2009, *J. Mar. Syst.*, *87*, 66–78.
Gibbs, R. J. (1974), Sediment transport model for Amazon River Atlantic Ocean, *Eos Trans. AGU*, *55*, 279–279.
Gordon, H. R., O. B. Brown, R. E. Evans, J. W. Brown, R. C. Smith, K. S. Baker, and D. K. Clark (1988), A semi-analytic radiance model of ocean color, *J. Geophys. Res.*, *93*, 10,909–10,924.
Harvey, M., J.-C. Therriault, and N. Simard (2001), Hydrodynamic control of late summer species composition and abundance of zooplankton in Hudson Bay and Hudson Strait (Canada), *J. Plankton Res.*, *23*, 481–496.

Hill, P. S., E. Boss, J. P. Newgard, B. A. Law, and T. G. Milligan (2011), Observations of the sensitivity of beam attenuation to particle size in a coastal bottom boundary layer, *J. Geophys. Res.*, *116*, C02023, doi:10.1029/2010JC006539.
Jonasz, M. (1983), Particle size distribution in the Baltic, *Tellus, Ser. B*, *35*, 346–358, doi:10.1111/j.1600-0889.1983.tb00039.x.
Kiefer, D. A., and J. Berwald (1992), A random encounter model for the microbial planktonic community, *Limnol. Oceanogr.*, *37*, 457–467.
Kostadinov, T. S., D. A. Siegel, and S. Maritorena (2009), Retrieval of the particle size distribution from satellite ocean color observations, *J. Geophys. Res.*, *114*, C09015, doi:10.1029/2009JC005303.
Kostadinov, T. S., D. A. Siegel, S. Maritorena, and N. Guillocheau (2012), Optical assessment of particle size and composition in the Santa Barbara Channel, California, *Appl. Opt.*, *51*(6), 3171–3189, doi:10.1364/AO.51.003171.
LISST-100X Particle Size Analyzer (2013), *User's Manual Version 5.0*, Sequoia Sci. Inc., Bellevue, Wash.
Loisel, H., and A. Morel (1998), Light scattering and chlorophyll concentration in case 1 waters: A re-examination, *Limnol. Oceanogr.*, *43*, 847–858.
Loisel, H., J.-M. Nicolas, A. Sciandra, D. Stramski, and A. Poteau (2006), Spectral dependency of optical backscattering by marine particles from satellite remote sensing of the global ocean, *J. Geophys. Res.*, *111*, C09024, doi:10.1029/2005JC003367.
Loisel, H., X. Meriaux, J. F. Berthon, and A. Poteau (2007), Investigation of the optical backscattering ratio of marine particles in relation to their biogeochemical composition in the eastern English Channel and southern North Sea, *Limnol. Oceanogr. Methods*, *52*(2), 739–752.
Maffione, R. A., and D. R. Dana (1997), Instruments and methods for measuring the backward-scattering coefficient of ocean waters, *Appl. Opt.*, *36*, 6057–6067.
Marrari, M., C. Hu, and K. Daly (2006), Validation of SeaWiFS chlorophyll a concentrations in the Southern Ocean: A revisit, *Remote Sens. Environ.*, *105*, 367–375.
Martinez-Vicente, V., P. E. Land, G. H. Tilstone, C. Widdicombe, and J. R. Fishwick (2010), Particulate scattering and backscattering related to water constituents and seasonal changes in the Western English Channel, *J. Plankton Res.*, *32*(5), 603–619.
Matsuoka, A., M. Babin, D. Doxaran, S. B. Hooker, B. G. Mitchell, S. Bélanger, and A. Bricaud (2014), A synthesis of light absorption properties of the Arctic Ocean: Application to semianalytical estimates of dissolved organic carbon concentrations from space, *Biogeosciences*, *11*, 3131–3147.
McKee, D., and A. Cunningham (2006), Identification and characterization of two optical water types in the Irish Sea from in situ inherent optical properties and seawater constituents, *Estuarine Coastal Shelf Sci.*, *68*, 305–316.
McKee, D., M. Chami, I. Brown, V.S. Calzado, D. Doxaran, and A. Cunningham (2009), Role of measurement uncertainties in observed variability in the spectral backscattering ratio: A case study in mineral-rich coastal waters, *Appl. Opt.*, *48*(24), 4663–4675.
Mikkelsen, O., and M. Pejrup (2001), The use of a LISST-100 laser particle sizer for in-situ estimates of floc size, density and settling velocity, *Geo Mar. Lett.*, *20*, 187–195, doi:10.1007/s003670100064.
Mikkelsen, O. A., T. G. Milligan, P. S. Hill, R. J. Chant, C. F. Jago, S. E. Jones, V. Krivtsov, and G. Mitchelson-Jacob (2008), The influence of schlieren on in situ optical measurements used for particle characterization, *Limnol. Oceanogr. Methods*, 6, 133–143.
Mobley, C. D., K. S. Lydia, and E. Boss (2002), Phase function effects on oceanic light fields. *Appl. Opt.*, *41*, 1035–1049.
Morel, A. (1973), Light scattering by seawater. Experimental results and theoretical approach, in *Optics of the Sea, AGARD-NATO (North Atlantic Treaty Organization) Lect. Ser.* No. 61, pp. 3.1.1–3.1.76, Neuilly-sur-Seine, France.
Morel, A., and S. Maritorena (2001), Bio-optical properties of oceanic waters: A reappraisal, *J. Geophys. Res.*, *106*, 7163–7180.
Neukermans, G., H. Loisel, X. Mériaux, R. Astoreca, and D. McKee (2012), In situ variability of mass-specific beam attenuation and backscattering of marine particles with respect to particle size, density, and composition, *Limnol. Oceanogr. Methods*, *57*, 124–144.
Pegau, W.S., D. Gray, and J. R. V. Zaneveld (1997), Absorption of visible and near-infrared light in water: The dependence on temperature and salinity, *Appl. Opt.*, *36*, 6035–6046.
Piskozub, J., D. Stramski, E. Terrill, and W. K. Melville (2004), Influence of forward and multiple light scatter on the measurement of beam attenuation in highly scattering marine environments, *Appl. Opt.*, *43*, 4723–4731.
Platt, T., and K. Denman (1978), The structure of the pelagic marine ecosystem, *Rapp. P. V. Reun. Cons. Int. Explor. Mer*, *173*, 60–65.
Proctor, C.W., and C. S. Roesler (2010), New insights on obtaining phytoplankton concentration and composition from in situ multispectral Chlorophyll fluorescence, *Limnol. Oceanogr. Methods*, *8*, 695–708.
Sheldon, R. W., A. Prakash, and W. H. Sutcliffe Jr. (1972), The size distribution of particles in the ocean, *Limnol. Oceanogr.*, *17*, 327–340.
Snyder, W., R. Arnone, C. Davis, W. Goode, R. Gould, and S. Ladner (2008), Optical scattering and backscattering by organic and inorganic particulates in US coastal waters, *Appl. Opt.*, *47*, 666–677.
St-Laurent, P., F. Straneo, J. F. Dumais, and D. G. Barber (2011), What is the fate of the river waters of Hudson Bay?, *J. Mar. Syst.*, *88*, 352–361.
Stramski, D. (1999), Refractive index of planktonic cells as a measure of cellular carbon and chlorophyll a content, *Deep Sea Res., Part I*, *46*, 335–351.
Stramski, D., and D. Kiefer (1991), Light scattering by microorganisms in the open ocean, *Prog. Oceanogr.*, *28*, 343–383, doi:10.1016/0079–6611(91)90032-H.
Stramski, D., E. Boss, D. Bogucki, and K. J. Voss (2004), The role of seawater constituents in light backscattering in the ocean, *Prog. Oceanogr.*, *61*, 27–56.
Sullivan, J. M., M. S. Twardowski, P. L. Donaghay, and S. A. Freeman (2005), Use of optical scattering to discriminate particle types in coastal waters, *Appl. Opt.*, *44*, 1667–1680.
Sullivan, J. M., M. S. Twardowski, J. R. V. Zaneveld, C. M. Moore, A. H. Barnard, P. L. Donaghay, and B. Rhoades (2006), Hyperspectral temperature and salt dependencies of absorption by water and heavy water in the 400–750nm spectral range, *Appl. Opt.*, *45*, 5294–5309.
Sun, D., Y. Li, Q. Wang, J. Gao, H. Lv, C. Le, and C. Huang (2009), Light scattering properties and their relation to the biogeochemical composition of turbid productive waters: A case study of Lake Taihu, *Appl. Opt.*, *48*(11), 1979–1989.
Twardowski, M. S., E. Boss, J. B. MacDonald, W. S. Pegau, A. H. Barnard, and J. R. V. Zaneveld (2001), A model for estimating bulk refractive index from optical backscattering ratio and the implications for understanding particle composition in case I and case II waters, *J. Geophys. Res.*, *106*, 14,129–14,142, doi:10.1029/2000JC000404.
Ulloa, O., S. Sathyendranath, and T. Platt (1994), Effect of the particle-size distribution on the backscattering ratio in seawater, *Appl. Opt.*, *33*, 7070–7077.
Van Heukelem, L., and C. S. Thomas (2005), The HPL method, in *The Second SeaWiFS HPLC Analysis Round-Robin Experiment (SeaHARRE-2), NASA TM/2005–212785*, edited by S. B. Hooker et al., pp. 86–92, NASA Goddard Space Flight Cent., Greenbelt, Md.
Werdell, P. J., C. W. Proctor, E. Boss, T. Leeuw, and M. Ouhssain (2013), Underway sampling of marine inherent optical properties on the Tara Oceans expedition as a novel resource for ocean color satellite data product validation, *Methods Oceanogr.*, *7*, 40–51.

Whitmire, A. L., E. Boss, T. J. Cowles, and W. S. Pegau (2007), Spectral variability of the particulate backscattering ratio, *Opt. Express*, *15*, 7019–7031.

Woźniak S. B., and D. Stramski (2004), Modeling the optical properties of mineral particles suspended in seawater and their influence on ocean reflectance and chlorophyll estimation from remote sensing algorithms, *Appl. Opt.*, *43*, 3489–3503.

Xi, H., P. Larouche, S. Tang, and C. Michel (2013), Seasonal variability of light absorption properties and water optical constituents in Hudson Bay, Canada, *J. Geophys. Res. Oceans*, *118*, 3087–3102, doi:10.1002/jgrc.20237.

Xi, H., P. Larouche, S. Tang, and C. Michel (2014), Characterization of variability of particle size distribution in Hudson Bay, Canada, *J. Geophys. Res. Oceans*, *119*, 3392–3406, doi:10.1002/2013JC009542.

Yentsch, C., and D. W. Menzel (1963), A method for the determination of phytoplankton chlorophyll and phaeophytin by fluorescence, *Deep Sea Res. Oceanogr. Abstr.*, *10*, 221–231.

Zaneveld, J. R. V., J. C. Kitchen, and C. M. Moore (1994), The scattering error correction of reflecting-tube absorption meters, *Proc. SPIE Ocean Opt. XII*, *2258*, 44–55.